Numerical modeling of curvilinear corrugated-core sandwich structures subjected to low velocity impact loading

***T. Boonkong[1,2], Y.O. Shen [3], Z.W. Guan[1] and W.J. Cantwell[4]**

[1] School of Engineering, University of Liverpool, L69 3GH, UK.
[2] Department of Engineering, The Royal Thai Naval Dockyard, Royal Thai Navy, Bangkok, Thailand
[3]School of Aerospace Engineering and Applied Mechanics, Tongji University, China
[4]Department of Aerospace Engineering, Khalifa University of Science, Technology and Research (KUSTAR), P.O. Box 127788, Abu Dhabi, United Arab Emirates

*Corresponding author: t.boonkong@liv.ac.uk

In this paper, simulations of low velocity impact characteristics of curvilinear corrugated-core sandwich structures were presented, which were validated against the corresponding experimental data. Two different configurations of lightweight aluminium sandwich panels from Metawell® Company in Germany were tested using drop-weight impact tower with spherical indenter to evaluate their energy-absorbing characteristics and to identify the associated failure mechanisms under vary of impact loading conditions.

Here, two panel configurations were studied based on the finite element analysis by using commercial finite element code Abaqus/Explicit developing numerical models to cover the most representative cases. A good degree of correlation was obtained, which indicates the finite element models developed are capable of predicting the dynamic behaviour of the curvilinear corrugated-core sandwich structure panels subjected to low velocity projectile impact.

Keywords: Curvilinear corrugated-core sandwich structures, low velocity impact, finite element, perforation failure.

Introduction

Sandwich structures are considered as optimal designs for a wide range of applications such as insulated structures, marine construction, transportation and aerospace vehicles. A composite sandwich panel is usually made from a lightweight foam, honeycomb or corrugated core sandwiched between two composite face sheets. Such a combination offers exceptional specific strength-to-weight ratio or stiffness-to-weight ratio, buoyancy, dimensional stability, and thermal and acoustical insulation characteristics. The curvilinear corrugated-core sandwich structure is one of outstanding sandwich structures offering superior mechanical properties. Many researches have been study on various types of sandwich structures [Biancolini (2005) , Nyman and Gustafsson (2000) , Rejab and Cantwell (2013) , Herrmann, Zahlen (2005) , Kazemahvazi and Zenkert (2009) , Xiong, Ma (2011) , Lin, Liu (2007) , Zenkert (1995) , Zhang Y (2011) , Yokozeki, Takeda (2006)]. However, it was found that few of published worked involved in curvilinear corrugated-core sandwich structures in spite of a versatile applications.

In this paper, the curvilinear corrugated-core sandwich structures from Metawell® company, which is a patented lightweight construction aluminium panel made by bonding two cover sheets to the core material, consisting of wave formed sheet metal, using a hot melt adhesive in a continuous, process were used and tested in order to study the influence of low velocity impact attached by the spherical indenter response to the rigid panels.

Experimental Work

The curvilinear corrugated-core sandwich structures in this study were based on EN AW-1582 H48 aluminium alloy sheets from fabricated by bonding two cover sheets into core material, which consists of wave formed sheet metal, using a hot melt adhesive in a continuous process. There were two panel configurations, which different fact sheet thicknesses and core sizes were tested. Fig.1 shows a design and dimension of both panels.

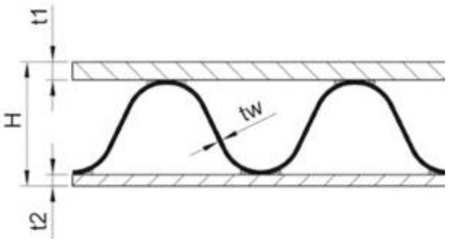

t_1 - thickness of top cover sheet

t_w - thickness of corrugation

t_2 - thickness of bottom cover sheet

H - panel height in mm.

Fig.1 shows a design and dimension of both panels.

Table 1. Panel dimensions

Type	t1 (mm)	t_w (mm)	t_2 (mm)	H (mm)	weight (kg/m^2)	Descriptions
Alu hl 05-02-05 hl/H6	0.5	0.2	0.5	6.0	3.8	lightweight panel (primer coated)
Alu cc 08-03-05 hl/H10	0.8	0.3	0.5	10.0	5.2	White coating on one side

Low velocity impact tests on the panels started from 1.93 m/s and increased gradually until 5.4m/s were conducted by using an Instron CEAST 9350 drop tower machine. A cylindrical impactor of 5.32 kg with 25.4 mm diameter spherical end was used. The test specimens had the dimension 155 mm. x 155 mm. The specimens were clamped by cylindrical ring with inside and outside diameter of 76 and 100 mm. respectively. The 200 N. of clamp force between both bottom and top rings was applied. Details about the test configuration are shown in Figure 2.

In order to get the materials properties for the input parameters used in finite element modelling, the top and bottom face sheets were tested by using Instron 4505 to conduct the uniaxial tensile test. The result from tensile test is shown as the graph in Fig. 3.

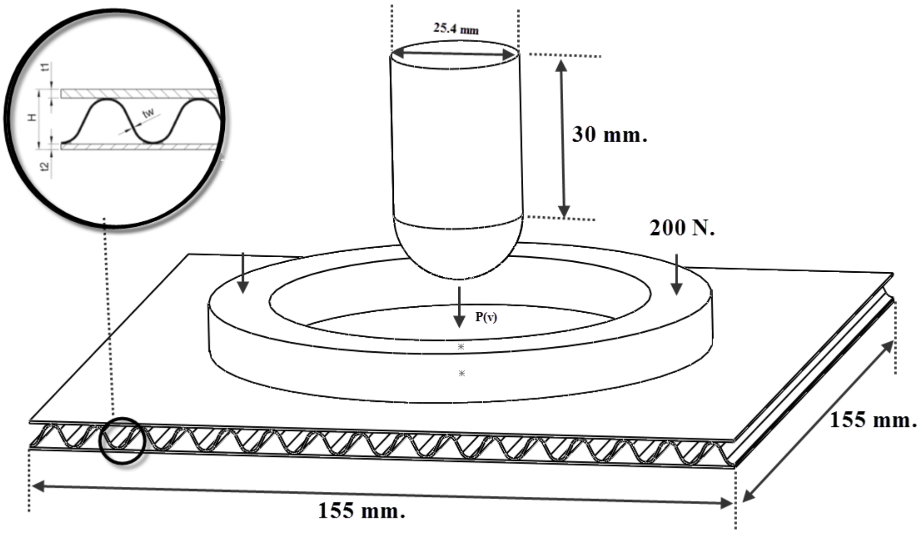

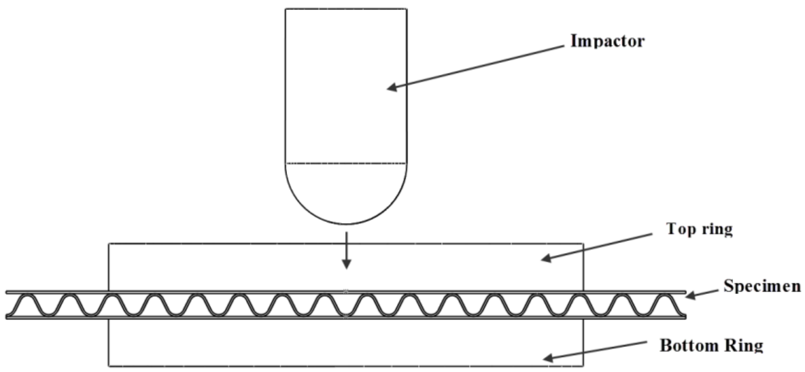

Fig.2 (a) Schematic of drop-weight apparatus, using spherical impactor (b) side view

Finite element modelling

ABAQUS/Explicit [Abaqus6.12-3 (2012)]was used to develop numerical simulations of the curvilinear corrugated-core sandwich structures under low velocity impact. The aluminium alloy was modelled as an elasto-plastic material with rate-dependent behaviour. For a rate-dependent material, the relationship follows the uniaxial flow rate definition as:

$$\dot{\bar{e}}^{pl} = h(q, \bar{e}^{pl}, \theta) \tag{1}$$

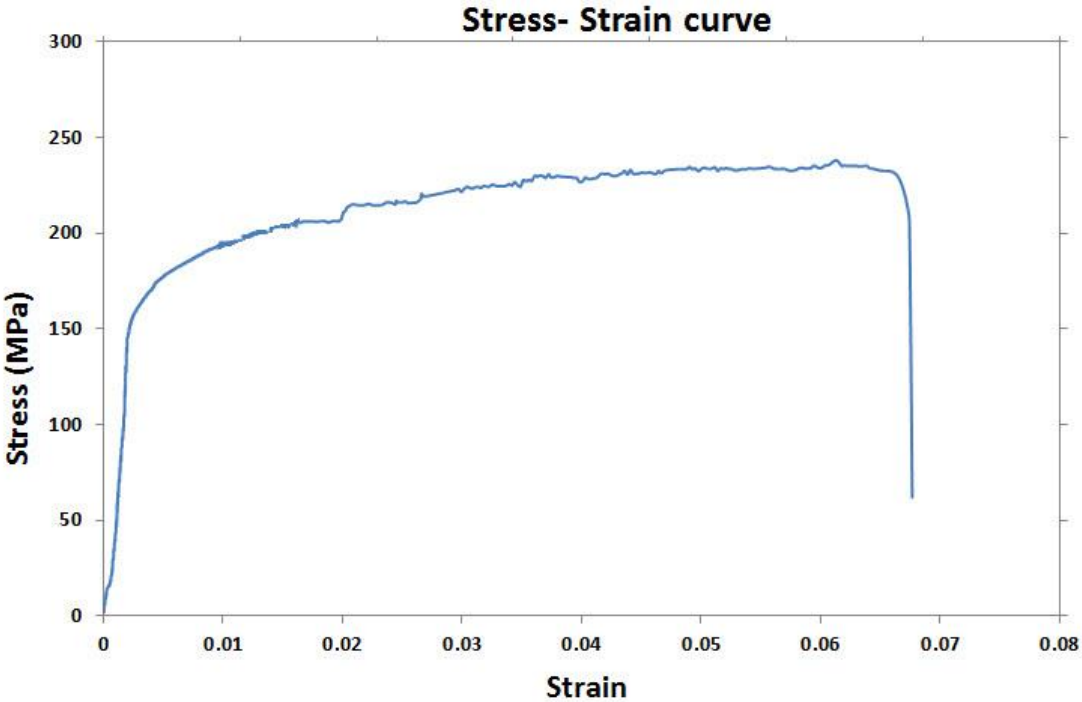

Fig.3 The stress- strain curve of EN AW-1582 H48 from tensile test

Where h is a known strain hardening function, q is the von-Mises equivalent stress, e^{-pl} is the equivalent plastic strain, and θ is the temperature. The isotropic hardening data for the EN AW-1582 H48 aluminium alloy are given in Table 2. The density of the aluminium was taken as ρ = 2690 kg/m^3. The material properties of EN AW-1582 H48 can be found in table 3.

Table 2. Isotropic hardening data for the EN AW-1582 H48 aluminium alloy

Yield stress (MPa)	153	160	178	203	214	224	231	234	235	232
Plastic strain	0	4E-4	0.002	0.013	0.020	0.030	0.040	0.050	0.056	0.065

The rate-dependent hardening curves can be expressed as:

$$\bar{\sigma}(\bar{\varepsilon}_{pl}, \dot{\bar{\varepsilon}}_{pl}) = \delta_y(\bar{\varepsilon}_{pl}) R(\dot{\bar{\varepsilon}}_{pl}) \quad (2)$$

Where $\bar{\varepsilon}_{pl}$ and R are the equivalent plastic strain and stress ratio (= $\bar{\sigma} / \sigma_y$) respectively.

Damage initiation criteria

Ductile damage criterion is a phenomenological model for predicting the onset of damage due to nucleation, growth, and coalescence of voids. The model assumes that the equivalent plastic strain at the onset of damage, $\bar{\varepsilon}_D^{pl}$, is a function of stress triaxiality and strain rate:

$$\bar{\varepsilon}_D^{pl}(\eta, \dot{\bar{\varepsilon}}_{pl}) \tag{3}$$

Where η = - *p/q* and η is the stress triaxiality, *p* is the pressure stress, *q* is the Misses equivalent stress, and $\dot{\bar{\varepsilon}}_{pl}$ is the equivalent plastic strain rate. The criterion for damage initiation is met when the following condition is satisfied:

$$\omega_D = \int \frac{d\,\bar{\varepsilon}_{pl}}{\bar{\varepsilon}_D^{pl}(\eta, \dot{\bar{\varepsilon}}_{pl})} = 1 \tag{4}$$

Where ω_D is a state variable that increases monotonically with plastic deformation. At each increment during the analysis the incremental increase is computed as:

$$\Delta\omega_D = \int \frac{\Delta\,\bar{\varepsilon}_{pl}}{\bar{\varepsilon}_D^{pl}(\eta, \dot{\bar{\varepsilon}}_{pl})} \geq 0 \tag{5}$$

Shear failure criterion

The shear failure model is based on the value of the equivalent plastic strain at element integration points; failure is assumed to occur when the damage parameter exceeds 1. The damage parameter, ω, is defined as :

$$\omega = \frac{\bar{\varepsilon}_0^{pl} + \sum \Delta\bar{\varepsilon}^{pl}}{\bar{\varepsilon}_f^{pl}} \tag{6}$$

where $\bar{\varepsilon}_0^{pl}$ is any initial value of the equivalent plastic strain, $\sum \Delta\bar{\varepsilon}^{pl}$ is an increment of the equivalent plastic strain, is the strain at failure, and the summation is performed over all increments in the analysis. The strain at failure, $\bar{\varepsilon}_f^{pl}$, is assumed to depend on the plastic strain rate, $\dot{\bar{\varepsilon}}_{pl}$; a dimensionless pressure-deviatoric stress ratio, *p/q* (where *p* is the pressure stress and *q* is the Mises stress); temperature; and predefined field variables. However, in this model, the temperature parameter would be ignored as a small effect to the results.

Element removal

When the shear failure criterion is met at an integration point, all the stress components will be set to zero and that material point fails. By default, if all of the material points at any one section of an element fail, the element is removed from the mesh; it is not necessary for all material points in the element to fail. For example, in a first-order reduced-integration solid element removal of the element takes place as soon as its only integration point fails. However, in a shell element all through-the-thickness integration points must fail before the element is removed from the mesh. In the case of second-order reduced-integration beam elements, failure of all integration points through the section at either of the two element integration locations along the beam axis leads, by default, to element removal[Abaqus6.12-3 (2012)].

Geometry and Mesh design

In order to reduce time of processing, only a quarter of modelling was generated. The Aluminium corrugated core and skin parts were meshed with a uniform mesh consisting primarily of 8-node linear brick, reduced integration, hourglass control elements (C3D8R). Core and skins were completely bonded with tie constrain around the interface areas. A 4-node 3-D bilinear rigid quadrilateral (R3D4) was used to contribute support rings and spherical end projectile.

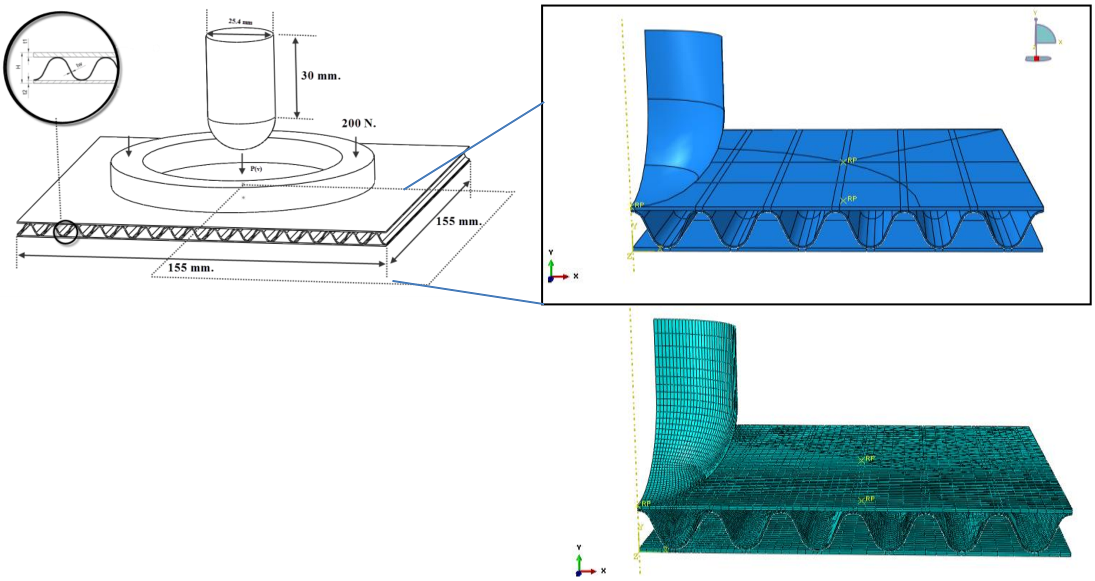

Fig.4 shows the quarter model assembly and mesh design.

Boundary conditions and loading

For the support bottom support ring, it was fixed all of degree of freedom and the -200 N. of uniform pressure was applied on the top support ring imitating as the experimental clamp condition. The projectile, which had the inertia of 5.321 kg, was allowed to translate only in y direction with the required predefined field of initial velocity.

The general contact, which had the contact domain included surface pairs by all with self-contact was applied for the whole model. The contact properties had frictionless tangential behaviour and hard contact for normal behaviour.

Table 3. Materials properties and parameters used in finite element modelling

Properties	Values
Young's modulus (Gpa.)	68
Density (kg/m^3)	2650
Strain rate	150
Fracture strain for ductile damage	0.065
Fracture strain for shear damage	0.050
Stress triaxiality	0.33
Fracture energy (kJ/m^2)	67

Results and discussions

Fig. 5 and 6 compare typical load-displacement plots for the impact energy from 10 J. up to 80 J. It could be indicated that the agreement between the experimental results

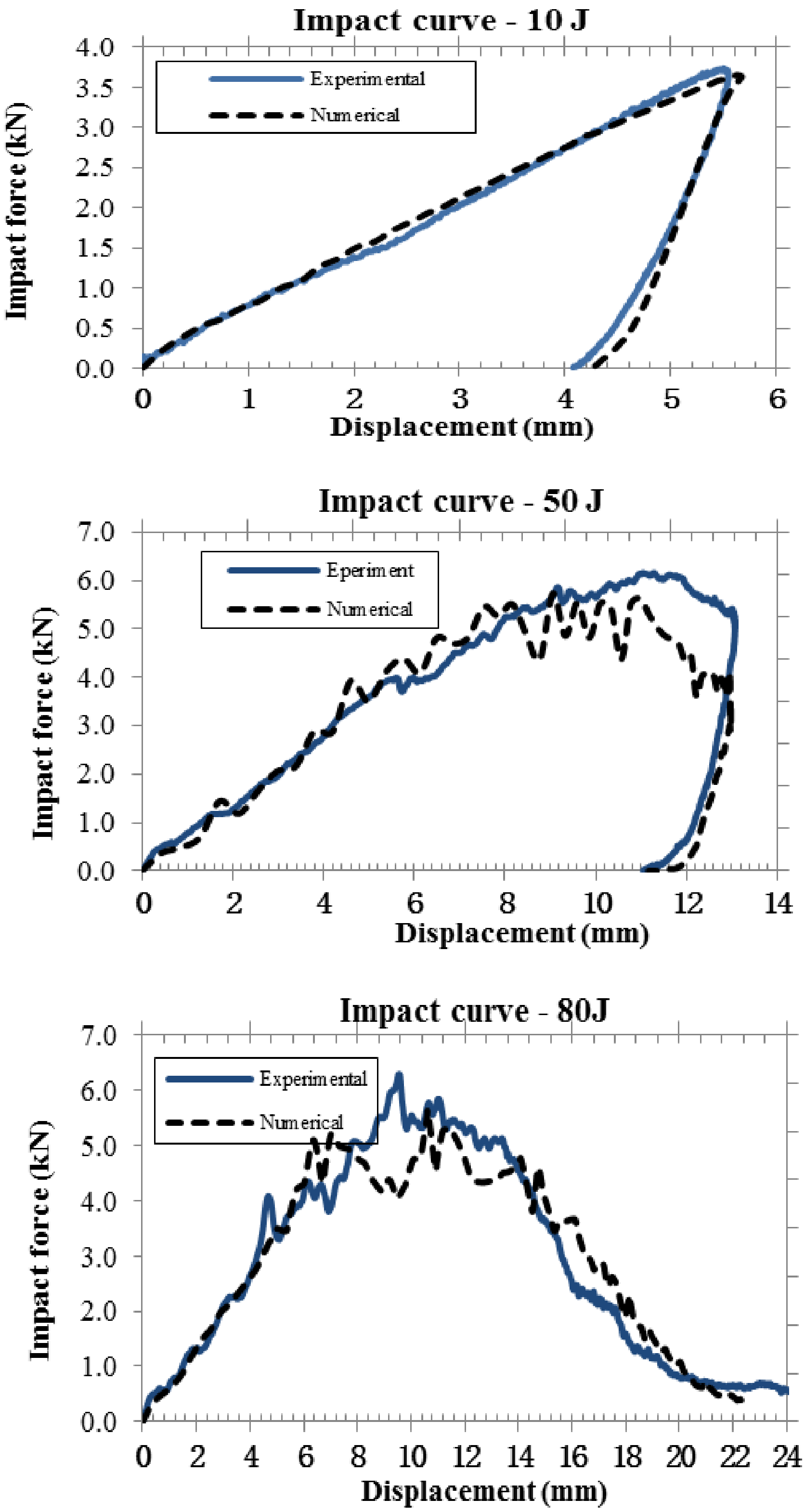

Fig. 5 Typical load-displacement plots from Alu hl 05-02-05 hl/H6 panels in ascending impact energy

and the numerical predictions is very good for both panels. For Alu hl 05-02-05 hl/H6, the prediction from numerical model slightly offered a higher impact displacement when 50J. was applied as shown in fig. 5. The results from numerical model seem be perforated slightly later than the experimental results according to the

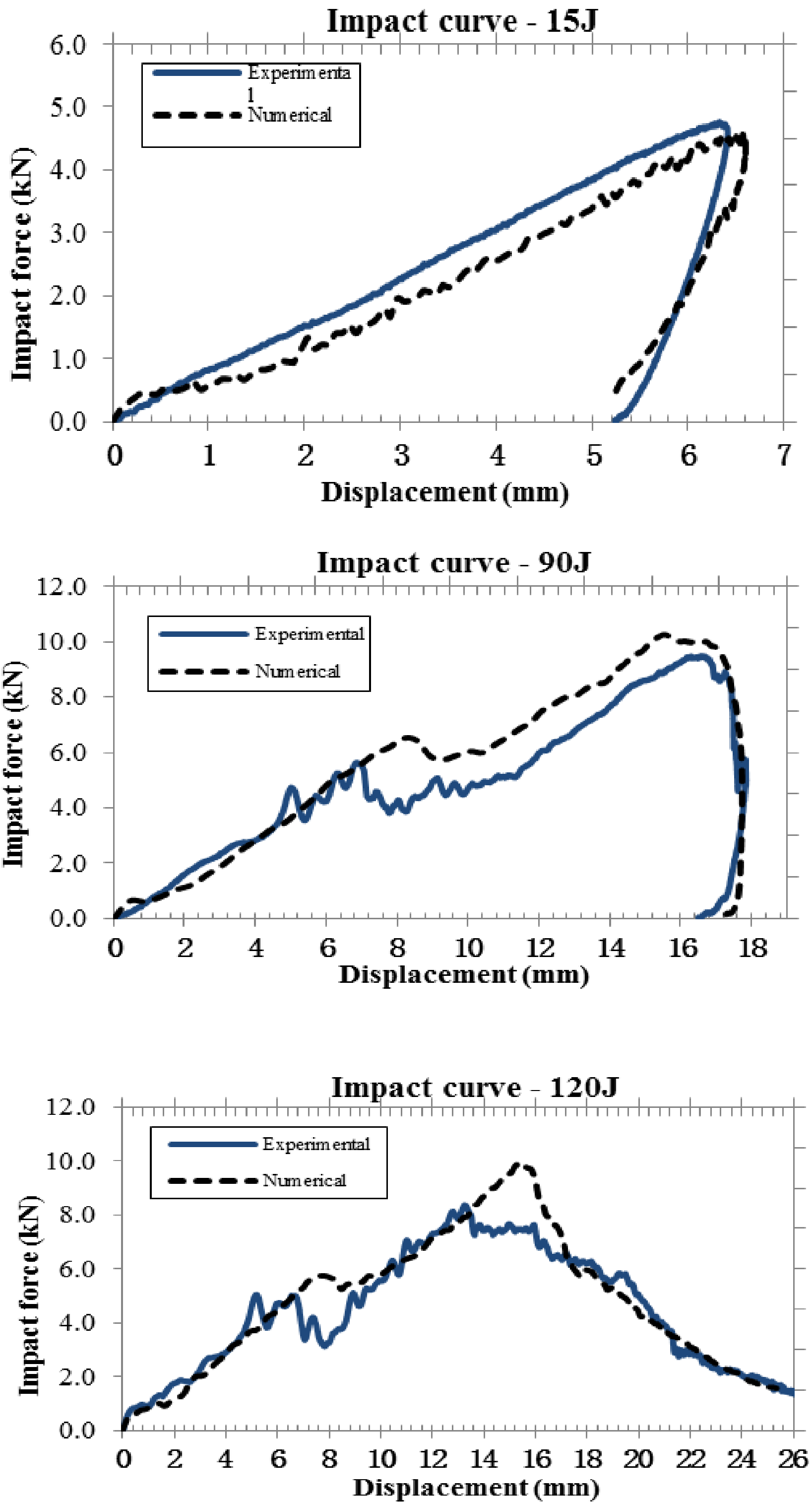

Fig. 6 Typical load-displacement plots from Alu cc 08-03-05 hl/H10 panels ascending impact energy

panel Alu cc 08-03-05 hl/H10 presented in fig. 6. Clearly, the peak load increases with the velocity. However, it was found that the panel Alu hl 05-02-05 hl/H6, which has less structures and bottom face sheet thickness, could offer a higher peak load in the range of velocity since 2.73 m/s to 3.8 m/s. It could be indicated that after 6 m/s, the bottom face sheet of Alu cc 08-03-05 hl/H10 obviously affected to the peak load as shown in fig. 7.

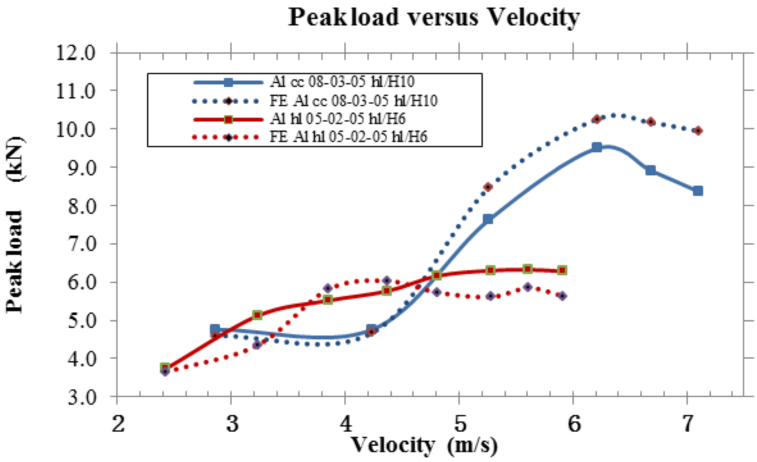

Fig. 7 compares peak load against velocity between panels Alu hl05-02-05 hl/H6 and Alu cc 08-03-05 hl/H10.

Apparently, the prediction offers correlation of peak load from Alu cc 08-03-05 hl/H10 in the initial state and it seem diverge when the velocity increased. Only in the range of 3.35 - 3.78 m/s from numerical results had slightly higher than the experimental results. It could be considered that the maximum perforation load is 9.4 kN. at 90 J. before dropping when increasing of velocity for Alu cc 08-03-05 hl/H10. Meanwhile, the trend of peak load seems to be constant while the impact velocity is increasing since 4.71 m/s.

From the finite element model results in fig. 8(c), it could gradually reveal the initial stress concentration and the propagation of failure on the panel since t = o millisecond until the panel was fully perforated at t = 6.00 milliseconds. It also could predict that the stress comes along the longitudinal corrugation direction (Z axis). The evidence revealed that it could not find the debonding failure mode between the corrugated-core and both top and bottom face sheets. Therefore, using the tie constrains between core and skins could be acceptable in the finite element model. It was found the buckling mode of failure mechanism occurred before the propagation of fracture would initiate. The initial crack did not propagate from the middle of impact, but started from the cavity inside the coalescent core then spread along z-direction as a crescent form.

The influence of projectile on the perforation resistance of the curvilinear corrugated-core sandwich structures are shown in fig. 8(a) and (b). Surprisingly, the diameter of penetration were investigated and found in double of the projectile diameter.

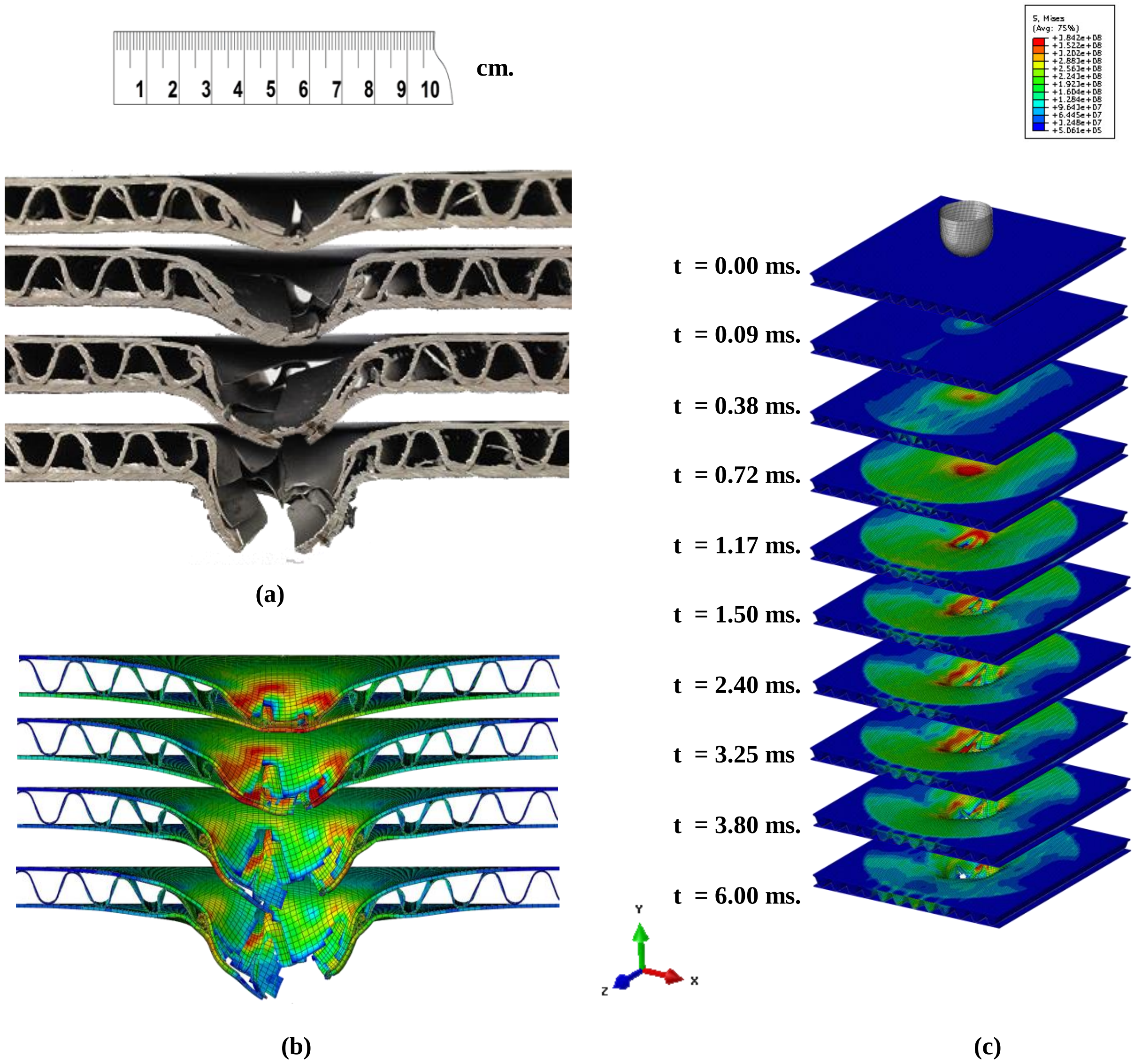

Fig. 8 (a) and (b) Compares central cross-section view of perforation between experimental and finite element modelling, using Alu hl 05-02-05 hl/H6, (c) Deformation of perforation since t = 0 millisecond until fully perforated at t = 6.00 millisecond.

Conclusions

Agreement between the experimental and predicted data is reasonably good, with the model tending to follow the experimental data. Only in some regions were observed not associated in particular the impact displacement, which seem offers slightly greater than measured data.

Increasing of the core and face sheets thickness enhances the stiffness and impact energy resistance quite in double of maximum peak load.

References

Biancolini, M.E. (2005), Evaluation of equivalent stiffness properties of corrugated board. Composite Structures, **69**(3): p. 322-28.

Nyman, U. and P.J. Gustafsson (2000), Material and structural failure criterion of corrugated board facings. Composite Structures, **50**(1): p. 79-83.

Rejab, M.R.M. and W.J. Cantwell (2013), The mechanical behaviour of corrugated-core sandwich panels. Composites Part B: Engineering, **47**(0): p. 267-77.

Herrmann, A., P. Zahlen, and I. Zuardy (2005), Sandwich Structures Technology in Commercial Aviation, in *Sandwich Structures 7: Advancing with Sandwich Structures and Materials*, O.T. Thomsen, E. Bozhevolnaya, and A. Lyckegaard, Editors., Springer Netherlands. p. 13-26.

Kazemahvazi, S. and D. Zenkert (2009), Corrugated all-composite sandwich structures. Part 1: Modeling. Composites Science and Technology, **69**(7–8): p. 913-19.

Xiong, J., et al. (2011), Mechanical behavior and failure of composite pyramidal truss core sandwich columns. Composites Part B: Engineering, **42**(4): p. 938-45.

Lin, Y.-K., et al. (2007), Fracture evolution in thick composites under compression. Polymer Composites, **28**(4): p. 425-36.

Zenkert, D. (1995) An introduction to sandwich construction / Dan Zenkert: Engineering Materials Advisory Services Ltd, 1995.

Zhang Y, Z.S., Wang Z. (2011), Crush behavior of corrugated cores sandwich
panels. Advanced Materials Research, **217-218**: p. 1584-89.

Yokozeki, T., et al. (2006), Mechanical properties of corrugated composites for candidate materials of flexible wing structures. Composites Part A: Applied Science and Manufacturing, **37**(10): p. 1578-86.

Abaqus6.12-3 (2012), Analysis User’s Manual. Dassault Systemes Simulia Corp. .